Deep Learning-Powered Lung Cancer Diagnosis: Harnessing IoT Medical Data and CT Images

Xiao Zhang[1], Xiaobo Wang[2], Tao Huang[3], Jinping Sheng[4]*
Department of Radiology, The General Hospital of Western Theater Command, Chengdu 610083, Sichuan, China[1, 4]
Emergency Medicine Department, The General Hospital of Western Theater Command, Chengdu 610083, Sichuan, China[2, 3]

***Abstract*—Currently, lung cancer poses a significant global threat, ranking among the most perilous and lethal ailments. Accurate early detection and effective treatments play pivotal roles in mitigating its mortality rates. Utilizing deep learning techniques, CT scans offer a highly advantageous imaging modality for diagnosing lung cancer. In this study, we introduce an innovative approach employing a hybrid Deep Convolutional Neural Network (DCNN), trained on both CT scan images and medical data retrieved from IoT wearable sensors. Our method encompasses a CNN comprising 22 layers, amalgamating latent features extracted from CT scan images and IoT sensor data to enhance the detection accuracy of our model. Training our model on a balanced dataset, we evaluate its performance based on metrics including accuracy, Area under the Curve (AUC) score, loss, and recall. Upon assessment, our method surpasses comparable approaches, exhibiting promising prospects for lung cancer diagnosis compared to alternative models.**

***Keywords*—Diagnosis; CT images; deep learning; convolutional neural network; lung cancer**

I. Introduction

The rising incidence of pulmonary ailments in contemporary industrialized societies underscores the urgent requirement for innovative models facilitating early and precise detection. Lung cancer, among these maladies, stands out as one of the most formidable cancers, contributing to a third of all cancer-related fatalities [1]. Consequently, it holds the grim distinction of being the deadliest and most hazardous cancer. Following diagnosis, approximately 80% of patients face a five-year survival prognosis, highlighting the severity of this disease. Air pollution ranks among the primary catalysts for lung cancer development [2]. Early detection of lung diseases significantly impacts the likelihood of successful treatment. Diagnosis typically involves a range of methods, including imaging modalities such as radiography, CT scans, biopsy, chest mucosa tests, and bronchoscopy. Lung nodules, characterized as small, round, and hazy masses within lung tissue, are radiographic opacities with diameters less than 30 millimeters [3, 4].

Enhancing the performance of CNNs involves incorporating task-specific layers tailored to the desired application. CNN models mimic certain aspects of human visual processing, thus enabling effective image analysis akin to human brain functions [5]. Consequently, extensive research has focused on utilizing CNNs for the automatic classification of lung cancer nodules from CT images. However, traditional CNN architectures typically rely solely on CT image features, neglecting potential contributions from physiological data that could enhance lung cancer diagnosis [3]. Conversely, advancements in medical IoT methodologies have facilitated remote patient monitoring, leveraging wearable health sensors. These sensors monitor various vital signs including blood pressure, body temperature, heart rate, respiratory patterns, weight fluctuations, and sleep behaviors [6, 7]. Notably, certain indicators such as anorexia, anxiety, constipation, depression, and fatigue pose challenges for direct tracking via wearable sensors [8].

However, there are alternative approaches that utilize textual and graphical interactions through mobile applications, offering symptom-based data that can aid in diagnosing lung cancer [9, 10]. This study introduces a medical body area network integrating medical IoT technologies and mobile applications. A data normalization technique, facilitated by the application programming interface, is employed to receive and process the data. Subsequently, the processed data is stored in a database using a relational schema.

Various studies have been conducted to identify and characterize lung diseases. Due to the abundance and complexity of lung radiographic images, distinguishing nodules from veins, wounds, and other structures poses a significant challenge for medical practitioners [4]. Computer-aided diagnosis systems serve as valuable tools to assist physicians in disease diagnosis. This paper introduces a novel approach based on a hybrid Deep Convolutional Neural Network (DCNN), trained on CT scans and medical data obtained from wearable IoT sensors. Our method incorporates a CNN with 22 layers, leveraging hidden features extracted from both CT images and IoT sensor data to enhance detection accuracy. Training our model on a balanced dataset, we evaluate its performance based on accuracy, Area Under the Curve (AUC) score, loss, and recall metrics.

The motivation behind this study stems from the pressing need for improved methods of early detection and precise diagnosis of lung cancer, given its significant impact on public health. With lung cancer accounting for a substantial portion of cancer-related deaths globally, there is an urgent requirement for innovative models that can aid in early detection, thereby improving treatment outcomes and patient survival rates. Traditional diagnostic methods, while effective to some extent, often rely solely on imaging modalities and may overlook valuable physiological data that could enhance diagnostic accuracy. Moreover, advancements in medical IoT technologies offer opportunities for remote patient monitoring, presenting a wealth of physiological data that could be leveraged for improved lung cancer diagnosis. By integrating

these disparate data sources and utilizing advanced machine learning techniques, using the DCNN, this study seeks to develop a novel approach that enhances the accuracy and efficiency of lung cancer detection, ultimately contributing to improved patient care and outcomes.

The subsequent sections of this article are structured as follows: Section II presents a literature review. Section III provides a detailed description of our proposed method. Section IV outlines the dataset used, tests performed, and results obtained. Finally, Section V offers conclusions and recommendations.

II. Related Works

Considerable progress has been made in lung cancer diagnosis, with numerous studies contributing to this field. In this section, we provide an overview of some notable research endeavors.

In study [11], researchers utilized Artificial Neural Network (ANN) techniques to analyze chest radiograph images for lung cancer detection. Their approach involved a novel method for identifying lung cancer from raw X-ray images sourced from the JSRT database. Initially, conventional image processing techniques were employed to reduce noise and differentiate lung structures from other anatomical features present in chest X-rays. Subsequently, regions displaying characteristics indicative of pulmonary nodules were isolated from the images. These areas were then subjected to statistical analysis, with the first and second categories of tissue statistical characteristics serving as input for ANN training. This process aimed to ascertain whether the identified regions represented nodules in the initial stage of diagnosis.

In study [12], the authors explored the use of CNN with transfer learning for the diagnosis of non-nodules, benign nodules, and malignant nodules, along with determining nodule locations. The experiments have shown that this proposed model has less ability in the characterization of the nodules of the benign and the nodules of malignant, and it is also unable to determine the exact location of the nodule. In study [13], the authors have used the K-nearest neighbor classifier in their proposed system. This classification identifies the K-nearest neighbor among all nodule candidates by searching in the feature space. Finally, the probability of nodule detection will be $\frac{n}{K}$, where n displays the number of the real nodules between K adjacent neighbors. They have stated in their article that the classification results are largely independent of the number of neighbors.

In study [14], a method combining features derived from wavelet transform and morphological characteristics was employed as input for Multilayer Perceptron (MLP). The number of neurons in the first layer of MLP depended on the input feature count, with neuron outputs determining whether a candidate region represented a nodule or normal tissue while neural networks excel in training based on explicit error criteria such as mean square error, direct comparison of network efficiency remains challenging. Neural networks suffer from the time-intensive nature of their training phase, exacerbated by the random selection of initial weights that are adjusted during learning, leading to varying separation thresholds. Thus, achieving an optimal configuration necessitates running the network multiple times with different initial weights and evaluating efficiency criteria.

In study [15], a combination of Artificial Neural Networks (ANN) and fuzzy clustering was employed for lung cancer diagnosis using CT scan images. Their model comprised four stages: pre-processing, target area evaluation, feature extraction, and final classification using ANN. Pre-processing involved various image enhancement techniques to enhance tumor observations in CT scan images. Subsequently, the target area was identified, and its features were input into the classification phase for diagnosis.

In study [16], the authors have presented a model based on the automata of cellular learning to detect cancer of the lung by using CT scan images. Their images contain both undesirable and significant features crucial for processing. In this framework, they employed pre-processing techniques, such as Gabor filtering, to enhance CT scan images. Images from prior stages were fed into the cellular learning automata for training, followed by extraction of automata rules. In study [17], the classification of the tumor tissue by using recurrent networks along with short-term memory is presented. The training samples are obtained from the real soft tissue samples through the tomography, and they are given as the input to the network. Their tests show that this classifier is a good choice for the classification. In study [18], authors utilized a combination of two-dimensional and three-dimensional models for pulmonary nodule detection, resulting in reduced false positive errors.

In study [19], the authors have used the model of ANN and the clustering of the fuzzy to detect the cancer of the lung. They have used two methods of the Hopfield neural networks and the clustering fuzzy algorithm to segment the color images. The experiments have displayed which ANN of Hopfield outperforms for the classification from the fuzzy clustering. In [20], the convolutional neural network with a cut has been used to diagnose the nodules of the pulmonary by the images of CT. The difference between their model and the traditional CNN model is in the use of a creative aggregation function. In [21], the main focus was on the feature extraction from the 3D CT images, and for this purpose, the morphological operators were used to thin the images. The classifier used in study [21] was the support vector machine. In study [22], to extract the feature, the embedded linear local maps have been used and correlation coefficients have been used to adjust the distance criterion in LLE.

The existing research landscape in lung cancer diagnosis reveals a plethora of methodologies, each with its strengths and limitations. However, a critical gap exists in the current literature, prompting the need for further investigation. While previous studies have explored various techniques, including ANN, CNN, and hybrid models, each approach has encountered challenges in accurately diagnosing lung cancer nodules. For instance, while ANN methods have shown promise in analyzing chest radiograph images, they may struggle with the precise identification of nodules due to limitations in feature extraction. Similarly, CNN models, despite their success in image classification tasks, may lack the ability to accurately determine nodule locations or characterize

benign versus malignant nodules. Moreover, techniques such as fuzzy clustering and cellular learning automata have demonstrated potential, yet their effectiveness in addressing the complexities of lung cancer diagnosis remains uncertain. Thus, there is a pressing need for novel methodologies that address these limitations, offering improved accuracy, robustness, and efficiency in lung cancer detection. This research gap underscores the motivation for the present study, which seeks to develop an innovative approach leveraging medical IoT data and advanced CNN architectures to enhance the accuracy and reliability of lung cancer diagnosis.

III. Our Presented Approach

Our method integrates CNN with medical IoT sensors, establishing a medical body area network that furnishes vital data for classification purposes. This approach significantly bolsters the reliability and precision of diagnosis. Following initial classification, identified nodules undergo segmentation, with subsequent sub-classification based on nodule size. This method typically unfolds in four sequential steps. Firstly, data collection entails transmitting sensor data from wearables and CT scanners to a central server. Next, data undergoes processing to train the network, encompassing numerical data processing and image data processing. In numerical data processing, data are condensed and outliers are identified and removed. Meanwhile, image preprocessing is performed to enhance features by minimizing the feature distance between cancerous and non-cancerous nodules. Subsequently, sub-classification based on nodule size ensues. The final step entails detection and decision-making based on predictions generated by our trained model.

It should be noted that the last conformity of the 5G technology in mobile has enabled advanced functionality of medical IoT sensors for the monitoring and the transmission of related data in real-time. These sensors can identify patient symptomatic information and send it to specified servers in real-time via the Internet. In the following and each of the below sub-sections, more details of our presented approach are provided.

A. First Step: Data Collection

As described, the medical IoT sensors form a network, depicted in Fig. 1(a). This network comprises sensors responsible for collecting physiological data. Communication within the network is structured into three levels, as illustrated in Fig. 1. Level 1 encompasses communication between sensors. Level 2 involves final devices utilized by patients for monitoring, accessing, and transmitting data to our proposed method. Level 3 manages the secure transmission of physiological data and CT images to the proposed method's server. Data collection occurs through two methods: active monitoring and passive monitoring. Active monitoring involves data collection via wearable IoT sensors, while passive monitoring involves patient interaction with sensors to generate data. This includes physiological data obtained through a mobile app and CT images. Level 2 networks comprise final devices utilized by patients, where physiological data is stored. Patients can access CT images through client-server communication. The server used in our proposed method receives data sent from the network at this stage.

In addition, the communication of the point of the access is maintained via the key of PreShared, it is applied as the main key of the pairwise in the 4 method-method handshakes [23]. Four thousand ninety-six iterations create PMK with 256 bits. The mentioned procedure exploits the function of the derivation of the key basis on the password, which is described in the relation as shown in Eq. (1):

$$PSK = PBKDF2\ (HMAC - SHA1.Password.SSID.4096.256) \quad (1)$$

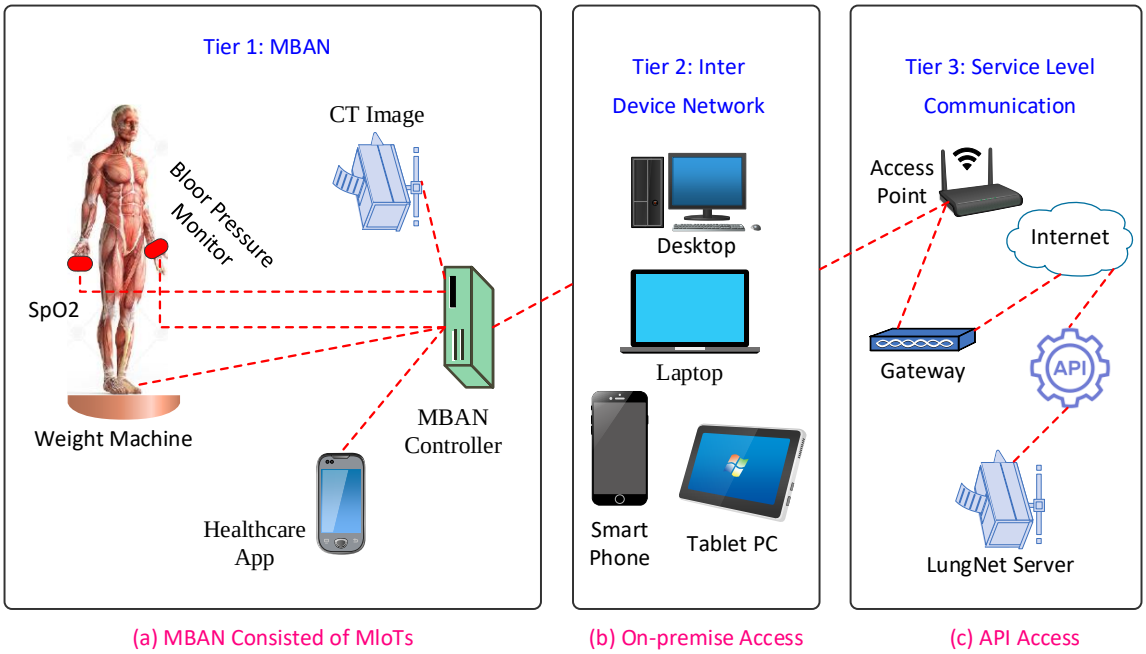

Fig. 1. The framework of the medical body area networkCT image.

A function of the Hash-based Message Authentication Code (HMAC) is applied for the generation of the hash of the password. On the mentioned test, the password has 16 characters, which are codified with the use of the ASCII of the printable. The counter of the packet and the service set identifier (SSID) are applied as the salt of the password. Then, the data is transmitted to the server with the patient's approval. The task manager checks the type of the data of the input. Next, the method schedules the tasks. Once data is placed in the database, the next stage is started. In these stages, the data is processed for the training, the validation, and the test of the model based on DNN. The data that is displayed by the portal of the patient doctor is also processed from this data.

B. Second Step: Pre-processing of Collected Data

The performance of Deep Neural Network (DNN)-based models relies heavily on both the quantity and quality of the data, emphasizing the importance of data preprocessing. Particularly, the focus lies on preprocessing imaging data related to lung cancer nodules, which often requires several stages of refinement. In this section, we outline the methods applied for preprocessing both non-image and image data.

Firstly, let's discuss non-image data preprocessing. Non-image data is typically gathered from sensor responses or patient interactions with healthcare applications. Wearable sensors capture various data such as temperature, irregular heartbeat, breathing patterns, and blood pressure. Additionally, non-wearable sensors are utilized for measuring weight loss and managing CT image data. Patient interactions also provide valuable data, including reports of anorexia, anxiety, depression, pain, insomnia, fatigue, and constipation. These signals and the relevant sensor values are normalized with the use of the defined linear normalization by relation as shown in Eq. (2). The lack of the related data is exchanged by NA. But, in the numerical calculations, these values are considered as 0. s' displays the normalized data, and s displays the real data.

$$s' = \frac{s - \min(s)}{\max(s) - \min(s)} \tag{2}$$

However, when dealing with image data, a distinct preprocessing approach becomes necessary. Image data processing comprises three main stages: 1) resizing and transforming the images; 2) validating candidate images; and 3) segmenting symmetrically with feature enhancement. Each Convolutional Neural Network (CNN) has a fixed input layer size, but there's no assurance that the input image size will align perfectly with the input layer size. Additionally, CNN input layers can only process a certain number of channels at a time. Hence, it's crucial to resize images and adjust color spaces according to network specifications. Certain CT scans may include regions with minimal lung tissue or even areas devoid of lung tissue entirely. Removing these sections improves the quality of training data.

Moreover, the ambiguous characteristics of lung cancer nodules pose challenges to the efficacy of feature learning layers. Consequently, it becomes imperative to augment the features of lung cancer nodules. The initial preprocessing step involves resizing images and transforming color spaces. The input layer size of our proposed model is set at 224×224×3. The collected data for this experiment includes both three-channel and one-channel images. All images are resized to 224×224 while maintaining the aspect ratio to streamline training duration. Furthermore, one-channel images are converted to RGB three-channel images using Eq. (3).

$$I_{RGB} = I_{(Gray.R)} + I_{(Gray.G)} + I_{(Gray.B)} \tag{3}$$

I_{RGB} represents our created RGB image from the grayscale image. Also, $I_{(Gray.R)}$, $I_{(Gray.G)}$ and $I_{(Gray.B)}$ represent, respectively, the equivalent value of the gray for the red channel, the equivalent value of the gray for the green channel, and the equivalent value of the gray for the blue channel. The size resizing of the image does not modify the data inside it due to the logical change. Even after the transformation of it into an image of 3-channel, our essential features stay without change. Our second processing of the image data is the candidate image validation. In this stage, the function of the validation takes the images. Then, it validates whether the image displays a candidate valid or not. The candidate's set of valid and set of invalids are shown in Fig. 2. If the image of the input does not include a part of the effective lung, which the nodules can be recognized, then the function ignores this image. Differently, this function rebounds the pre-processed copy of the image, and then, the algorithm exploits it for more pre-processing. This function takes the images of RGB (I_{Color}) which it is described as below:

$$I_{Color} = \sum_{n=1}^{N}\sum_{m=1}^{M} I(n.m.g) + \sum_{n=1}^{N}\sum_{m=1}^{M} I(n.m.r) + \sum_{n=1}^{N}\sum_{m=1}^{M} I(n.m.b) \tag{4}$$

Also, the image of RGB is transformed into an image of the grayscale by using relation, as shown in Eq. (5).

$$I_{gray}(n.m) = \alpha I_{Color}(n.m.r) + \beta I_{Color}(n.m.g) + \gamma I_{Color}(n.m.b) \tag{5}$$

α, β, and γ denote the constants for the red, green, and blue channels, respectively. It is essential to calculate the part area of the lung in the image because it is necessary to check whether I_{Color} is a valid candidate or not. It is easier and faster to measure the lung area in the binary image. The threshold of the gray conversion I_{gray} into the binary image is calculated by using the Otsu method, which is shown in the relation (6):

$$\sigma_b^2(t) = \sigma^2 - \sigma_w^2(t) = \omega_0(\mu_0 - \mu_T)^2 + \omega_0(\mu_1 - \mu_T)^2 \tag{6}$$

where, $\sigma_b^2(t)$ is the maximum threshold and σ^2 represents the variance and μ_0 represents the mean. Also, ω_0 is the weighted probability. The obtained threshold from the relation (6) is used to transform $I_{gray}(n.m)$ into a binary image $I_{bin}(n.m)$ by using the relation (7).

$$X = \begin{cases} 1 & I_{gray}(n.m) \geq \sigma_b^2(t) \\ 0 & otherwise \end{cases} \tag{7}$$

A binary image contains small noise objects that these objects have areas of about 450 -5000 pixels. The obtained

objects influence the accuracy of the learning of the layers of the learning of the feature. Thus, that is why it is essential to discard these cases. The opening of the region of the morphological is applied for the removal of the objects by a value of the threshold equal to 5000. The series of little holes remain in the foreground after the region opens. To remove the holes, the operation of the flood filling by the four-way connection is applied.

$$I_{fill}(n.m) = Flood_{filling}(area_{opening}(I_{bin}(n.m))) \quad (8)$$

where, $I_{fill}(n.m)$ displays the image after filling the holes and $I_{bin}(n.m)$ is the binary image. Next, the image of the binary is deduced by the filled image. Finally, it renders the lung form as an object in the foreground.

$$I_{sub}(n.m) = I_{fill}(n.m) - I_{bin}(n.m) \quad (9)$$

where, $I_{sub}(n.m)$ displays the image after the deduction of the image of the binary by the filled image. Then, the area is computed with the implementation of a logical operation of AND among $I_{sub}(n.m)$ and the logical 1, which is shown in the relation (10).

$$Area = \sum_{n=1}^{N}\sum_{m=1}^{M} I_{sub}(n.m) \wedge Logical(1) \quad (10)$$

Assuming the area exceeds 20,000, we consider the image to represent a valid candidate for lung cancer nodule diagnosis. Conversely, if the area falls below 20,000, the image is deemed invalid. Validating the candidate confirms the efficacy of the feature learning layer and captures key features crucial for lung cancer nodule classification. Thus, this method serves to enhance the quality of lung cancer image datasets.

Lastly, the third step in image data processing involves segmenting the lungs symmetrically and enhancing features. Following validation, symmetric segmentation is performed. The segmented lungs, enhanced by improved features, are illustrated in Fig. 3. The lung separation function operates on the pre-processed binary image copies of valid candidate images (I_sub(n.m)). At this stage, both the left and right lungs are presented in a composite image. To separate the left and right lungs, two separate masks need to be generated. This process initiates by convolving an image of zeros with the grayscale image and saving the results as left and right masks, as described in Eq. (11) and Eq. (12).

$$L_{mask} = \sum_{n=1}^{N}\sum_{m=1}^{M} I_{gray}(n.m) \otimes I_{zero}(n.m) \quad (11)$$

$$R_{mask} = \sum_{n=1}^{N}\sum_{m=1}^{M} I_{gray}(n.m) \otimes I_{zero}(n.m) \quad (12)$$

L_{mask} and R_{mask} indicate the mask of the left and the mask of the right. $I_{sub}(n.m)$ contains more than one area with the values of the pixel of the binary. For the segmentation of the obtained areas, it is necessary to label them. The labeling is performed with the use of the relation (13) where $K = \{x | x \in N\}$ and I_{str} is an 8-connection morphological structure with the pixel values equal to 1.

$$L_K = (L_{K-1} \otimes I_{str}) \cup I_{sub} \quad (13)$$

where, L_K is the label of the region K. Also, $I_{sub}(n.m)$ can have a maximum of two regions. That is why, $L_K = \{x \mid x \in N. x \leq 2\}$. In L_{mask} where $L_K = 1$, the values of the pixel are filled. In the same way, in R_{mask} where, $L_K = 2$, the values of the pixel are also filled. Finally, L_{mask} and R_{mask} are deduced by the main image to fill masks further. Next, the opening of the morphological with the ellipse has a main axis equal to 90 pixels and a height equal to 10 pixels. This case is used in 2 masks and the other complementary action, which is described by the relation (14). M_o displays the opening of the morphological and M_{mask} represents the mask of the left and the mask of the right.

$$X_{mask} = 1 - M_o((1 - X_{mask}).\frac{n^2}{90^2} + \frac{m^2}{10^2} \quad (14)$$

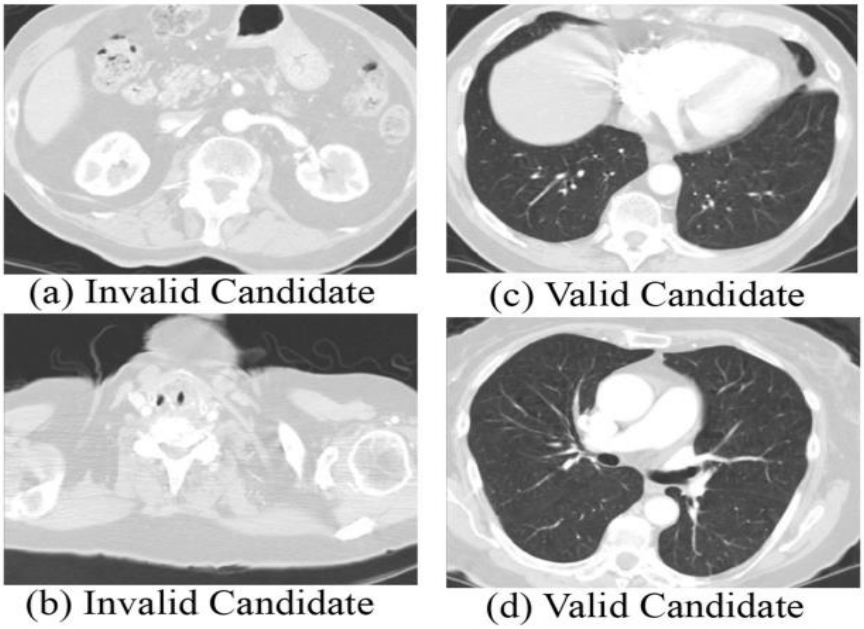

Fig. 2. (a,b) the candidates of the invalid; (c,d) the candidates of the valid.

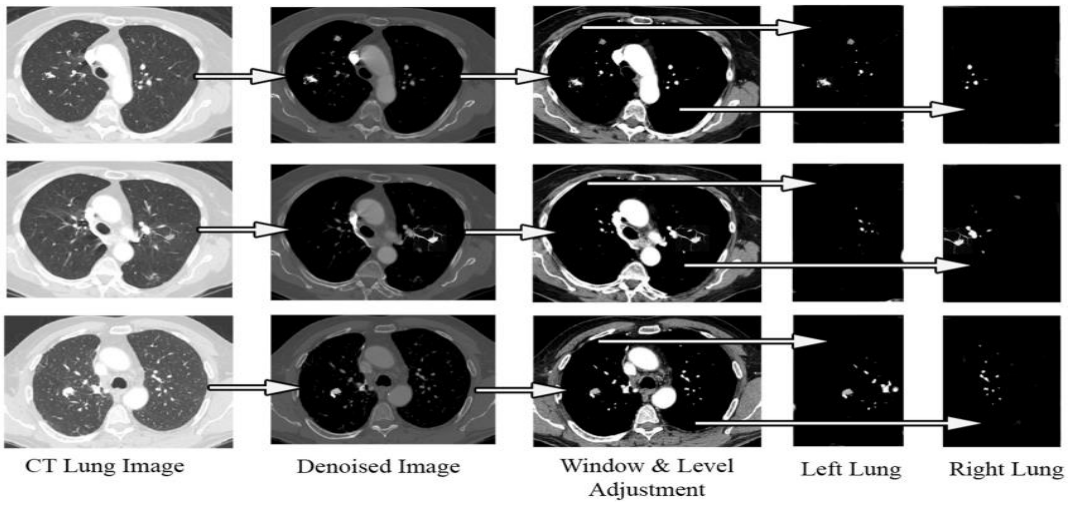

Fig. 3. The segmentation of the symmetric and the enhancement of the feature in the image data processing stage.

The obtained masks from the relation (14) include a blurred gradient. Binarization for X_{12} in the value of the threshold equal to 0.5 returns the severe discontinuities.

$$X_{mask} = \begin{cases} 1 & X_{mask} \geq 0.5 \\ 0 & otherwise \end{cases} \quad (15)$$

Finally, the masks are connected with $I_{sub}(n.m)$ as separately and then, it separates the lung of the left and the lung of the right from the image of the source.

$$I_{lung} = \sum_{n=1}^{N} \sum_{m=1}^{M} I_{gray}(n.m) \otimes X_{mask}(n.m) \quad (16)$$

Here, I_{lung} represents the lung of the left and the lung of the right separately. If $I_{gray}(n.m)$ is convolved by the mask of the left, relation (16) creates the left lung. Similarly, when $I_{gray}(n.m)$ is convolved with the right mask, the relation (16) creates the lung of the right. Finally, the lung of the left and the lung of the right are elided together.

The enhancement of the feature is a successive procedure that this procedure begins with noise removal. The non-local average methods, under the control of the relation (17), have been applied to the current test for the removal of the noise from the image, which in it, $\nu(I_f)$ displays the pixel of the filtered, $\nu(I_s)$ displays the pixel of the target and $\upsilon(I_s)$ represents the value of the unfiltered in $\nu(I_f)$. Also, $f(I_f.I_s)$ is the weighting function [24].

$$\nu(I_f) = \frac{1}{c(I_f)} \int_{n \times m} \upsilon(I_s) f(I_f.I_s) dI_f \quad (17)$$

Following noise removal, the adaptive histogram equalization algorithm, leveraging genetic algorithms [25], is applied. Subsequently, a surface contrast enhancement window is utilized to eliminate irrelevant features unrelated to lung cancer nodules. The segmentation result of the symmetric and the outcome of the feature enhancement process are depicted in Fig. 3. Augmenting data is one strategy employed to address overfitting challenges. However, the annotated dataset, even with input from radiologists, proves insufficient for achieving optimal classification efficiency in our model. Moreover, a significant disparity exists between the number of positive and negative training images, leading to imbalanced data in predictive modeling. To address this, we employ data augmentation techniques to generate additional relevant data from the existing dataset, thereby balancing the number of positive and negative images. Sufficient training samples are created through random spatial transformations and data augmentation methods.

C. Third Step and Fourth Step: Proposed Network, Training, and Classification

The proposed method introduces a unique network structure and a combined classification approach. This method employs a deep network with 22 layers, enabling it to learn distinctive features of lung cancer nodules. Additionally, the combined classifier enhances efficiency and provides more reliable predictions by leveraging data from the medical body area network. The CNN architecture used in our method is illustrated in Fig. 4, featuring a convolutional neural network with 22 layers and an input layer size of 224×224×3. Rectified Linear Unit (ReLU) functions are applied as activation functions for each convolution operation in the network.

Given the centralized server used by the network, reducing operational costs and maintaining accuracy presents a challenge. To address this, we adopt an alternative method compared to advanced CNN models, which typically utilize convolution operations of size n×n. Instead, our proposed model employs convolution operations of size 1×1, resulting in reduced weights and biases. However, this deepens the network model, leading to a performance reduction of 46%. It's worth noting that fully connected CNNs are popular among researchers in lung cancer diagnosis due to their satisfactory efficiency [26].

Nevertheless, a model of the fully connected needs further resources of computational from the models of the sparsely connected [27]. That is why, thus, in our proposed method, a model of the non-fully-connected is applied. In addition, a global layer of the average-pooling averages the signals; it decreases the 7×7 feature maps to the 1×1 feature maps to reduce the number of non-cooperative features.

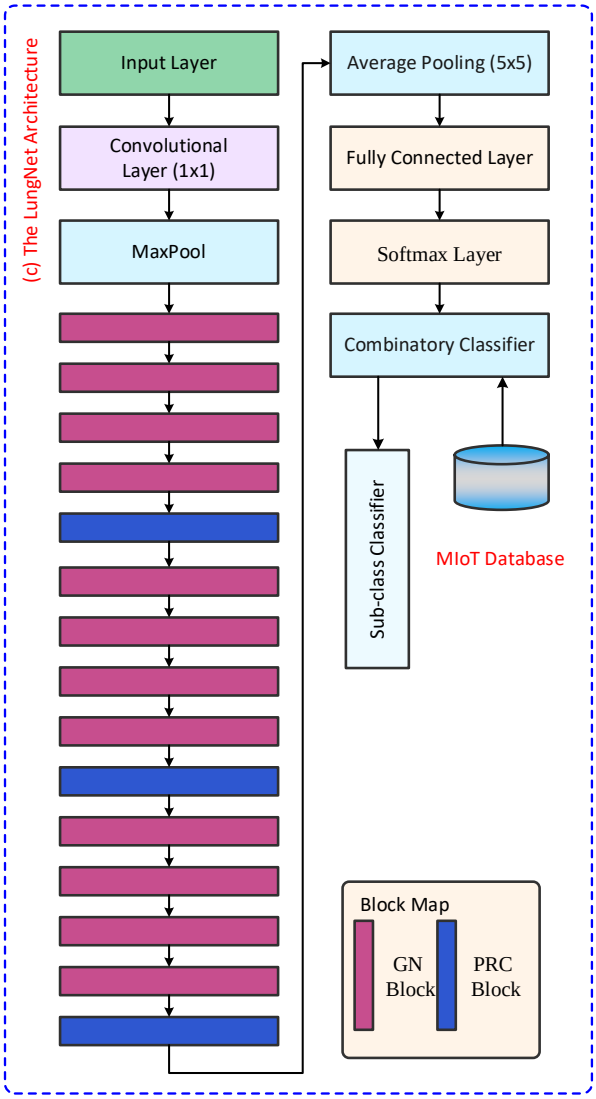

Fig. 4. Structure of the presented method.

It has been observed that employing a diverse range of convolutional matrices instead of a constant matrix enhances network performance. In our proposed method, convolutional matrices of sizes 1×1, 3×3, 5×5, and 7×7 are aggregated together by a max-pooling layer of size 3×3, which operates in parallel with this stack. The ability of the convolutional layer to investigate objects of varying sizes is crucial, and the use of multiple convolution matrices ensures this capability.

These separate layers are then combined into a deep concatenation layer, which transmits signals to the subsequent layer. In contrast to fully connected layers, our proposed method includes several intermediate pre-classification layers to mitigate the impact of the vanishing gradient problem. These branches are only activated during the training process. The purpose of these pre-classification layers is to perform classification before reaching the final classifier. Each of these layers comprises a 5×5 average pooling layer with a stride of 3, performing convolutions with 1×1 filters totaling 128 filters. The proposed method features 5 output nodes, processed through a softmax classification layer and aided by dataset data. The 2nd and 3rd nodes are combined for sub-classification.

In terms of the learning algorithm, it's worth noting that most CNNs initialize the weights of the classification layer randomly. However, for our proposed method, we've adopted various techniques to achieve better efficiency. Empirical results indicate that employing the modified Nguyen-Widrow initial weighting approach [28] improves validation accuracy and reduces validation loss more quickly.

We utilize the Levenberg-Marquardt backpropagation algorithm as the learning rule [29]. This choice is validated by the computational expense of calculating the Hessian matrix [30]. Given that our proposed method is intended to operate from a centralized server, multiple instances could degrade service quality. The Levenberg-Marquardt backpropagation algorithm estimates the Hessian matrix using the Jacobian matrix, which is computationally cheaper and faster [31]. Consequently, we update weights using the Levenberg-Marquardt backpropagation algorithm.

Furthermore, employing a dynamic learning rate, as opposed to a fixed learning rate, enhances validation accuracy [32]. Therefore, our proposed method adopts an adaptive learning rate during training, where the rate starts at 0.01 and gradually decreases to 0.0003.

After the training step, the classification step is done. A new hybrid classifier is designed and is used in the proposed method. The network classifier is considered for cancer classification. The data of the feature of the image of the high level and the data of the feature of the image of the low level are the features of the node based on the classification of the network. Commonly, the data of the probabilistic network is applied for the classification. Our proposed method incorporated an extra system of support for the decision-making of the weighted with the classifier of the convolution. The normalized data are the parameters of the step of the classification. The sum of the weighted of the prediction for our proposed method (P_L) and also prediction based on the normalized data (P_S), which is defined by the relation (18), form the final output of the proposed method.

$$P_{stage_n} = 0.6P_L + 0.4P_s \quad (18)$$

By using the value of P_{stage_n}, where $n = \{n \mid n \subset Z. 0 \leq n \leq 4\}$, the classification of the final (based on the medical thresholds) is performed. The lung cancer is further classified based on the size of the nodule. After the classification, the test image is sent to the sub-classifier. This module includes a module for the processing of the image and also a module for decision-making. The module of the processing of the image separates the nodule of the lung from the image. Next, the module of decision-making computes the nodule size. Based on the medical thresholds, this module classifies the nodules (see Fig. 5).

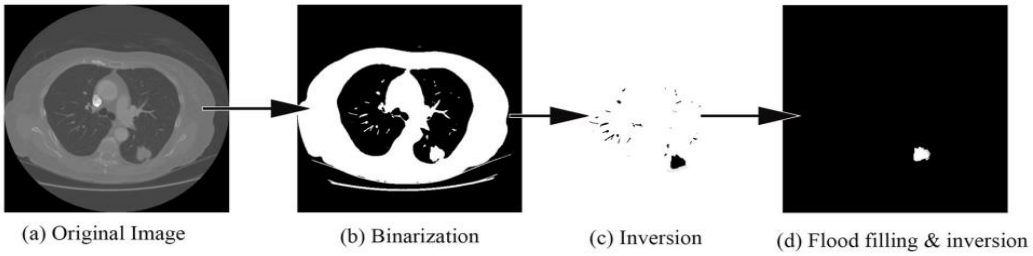

Fig. 5. An example of the separation of the lung nodule from the sub-classified image.

IV. Tests and Evaluation of Results

In this section, the details of the evaluation criteria, the used datasets, our performed tests, and the gained outcomes are provided. The language of the programming of Python has been applied to implement these experiments. Our proposed approach is done in a computer with 8G RAM and Core (TM) i7 CPU 3.0 GHz Intel(R). The network of the convolutional is implemented on GPU and the used card of the graphics in our approach is GEFORCE 840M for NVIDIA.

A. Applied Datasets and Evaluation Criteria

The performance evaluation criteria in this paper include accuracy, false positive rate, and false negative rate, which are utilized to calculate the Area Under the Curve (AUC) score and Recall. The LIDC-IDRI dataset [33] and the LUNGx dataset [34] are employed to evaluate the effectiveness of our proposed approach and to compare it with similar approaches. These two datasets are combined into a single dataset for evaluating our approach. Additionally, data obtained from the medical body area network are incorporated into this evaluation process.

Within this dataset, image scans containing lung regions are considered non-candidates and are consequently excluded from the datasets.

Furthermore, the datasets contain scans both with and without nodules. These cases are identified and separated based on existing metadata within the dataset, with annotations performed by radiologists. However, there is no inherent distribution logic between these two classes. Following partitioning, the number of images available for training, testing, and validation is insufficient. The scarcity of images poses a challenge in achieving satisfactory validation accuracy for CNNs. To overcome this challenge, we employ two-dimensional spatial image enhancement and generate features to preserve enhanced images using the existing dataset [35]. As a result, each CT scan is represented as a 3-channel image with dimensions of 224×224. The statistics of our utilized datasets are presented in Table I.

B. Obtained Results

In this section, we examine and also, we analyze the obtained results from the different experiments. Before the presentation of the results, we should mention that we compare the obtained outcomes by our presented approach with the obtained outcomes by the ResNet-50 network [36], the Inception V3 network [37], and the Xception network [38]. The results of our presented approach and other deep learning-based networks in our used dataset and the obtained data are provided in Tables II, III, and IV. Also, Fig. 6 displays the efficiency of deep learning models and the efficiency of our presented model according to accuracy, score of AUC, and loss. Note that in Tables II, III, and IV, results are presented for training, validation, and testing, respectively.

TABLE I. The Statistics of used Datasets and their Combination for the Evaluation of the Proposed Method

Dataset	CT Cases	Candidate Cases	Cases with Nodules	Augmented Cases
LUNGx	70	3280	1822	160000
LIDC-IDRI	1018	8252	5249	365000

TABLE II. Outcomes of Training of the Different Deep Learning Approaches and Our Presented Approach

Model	Accuracy	AUC Score	Recall	Loss
ResNet-50	99.56	99.99	99.60	0.045
InceptionV3	94.25	96.40	94.23	1.960
Xception	94.10	96.70	94.08	1.450
Proposed Model	99.85	100	99.76	0.0018

TABLE III. Outcomes of Validation of the Different Deep Learning Approaches and Our Presented Approach

Model	Accuracy	AUC Score	Recall	Loss
ResNet-50	84.20	94.90	83.50	0.598
InceptionV3	82.07	88.50	82.10	15.70
Xception	82.10	90.00	82.06	8.270
Proposed Model	92.25	98.12	91.54	0.324

TABLE IV. OUTCOMES OF TEST OF THE DIFFERENT DEEP LEARNING APPROACHES AND OUR PRESENTED APPROACH

Model	Accuracy	AUC Score	Recall	Loss
ResNet-50	84.13	94.85	83.45	0.604
InceptionV3	82.09	88.65	82.06	15.64
Xception	82.12	90.13	82.07	8.301
Proposed Model	92.78	98.46	92.01	0.321

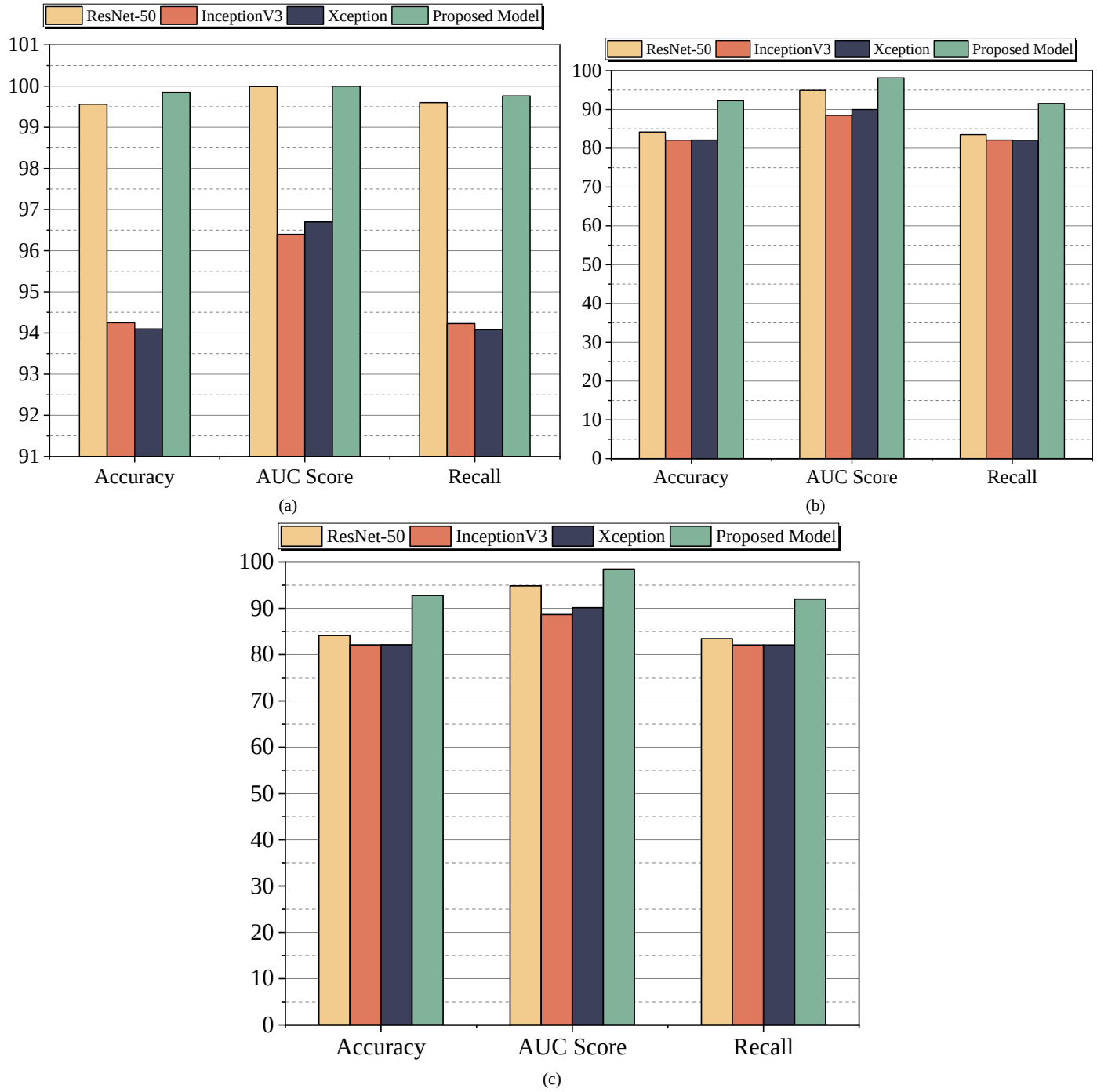

Fig. 6. Illustration of performance evaluation results for different methods, (a) Result of training process, (b) Result of validation process, (c) Result of test process.

After analyzing the outcomes of our proposed model and comparing them with ResNet-50, Inception V3, and Xception, it is evident that our model outperforms similar deep learning models, as shown in Tables II, III, and IV, as well as Fig. 6. Our proposed method achieved a test accuracy of 92.78%, a test AUC score of 98.46%, a test recall of 92.01%, and a test loss of 0.321.

In Fig. 6, the accuracy, AUC score, and loss values of different models are depicted. These metrics are crucial for evaluating model performance. Notably, our proposed model exhibits the highest test accuracy compared to other models. The AUC score is a key measure for assessing method efficiency and its ability to discriminate between positive and negative classes. A higher AUC score indicates superior performance. A score between 0.7 and 0.8 is considered acceptable, between 0.8 and 0.9 is excellent, and above 0.9 is considered outstanding [39]. As shown in Fig. 6, the proposed method not only achieved the highest test accuracy but also attained the highest test AUC score, indicating its excellent discriminatory ability between positive and negative classes.

Indeed, the loss value is another crucial criterion in assessing model performance. It represents the degree of inaccuracy in the model's predictions at each iteration. A loss value of 0 indicates perfect model predictions, whereas higher loss values indicate poorer performance. In our detection process, we use the cross-entropy loss function, commonly employed for multi-class classification tasks [38]. The proposed method achieves the lowest loss value, indicating superior predictive accuracy. Conversely, models such as Xception and Inception V3 exhibit significantly higher loss values [40, 41]. This evaluation demonstrates that our approach outperforms other deep learning models in diagnosing various types of lung cancer using the datasets and collected data.

C. Discussion and Limitations

Despite the promising results observed in various tests, the proposed method has several limitations, most of which are typical of CNN-based models. These limitations are outlined below.

Firstly, the efficacy of our approach, which surpasses that of similar methods, heavily relies on hybridization. The integration of data from the medical body area network contributes to the combined layer. However, any erroneous measurements by faulty IoT sensors could significantly compromise the overall integrity of the model. Although such occurrences are rare, the absence of a fault detection mechanism for medical sensors poses a potential risk.

Moreover, like any lung cancer classifier based on CNN, our proposed method requires image processing to enhance features. This image processing involves a series of computationally expensive processes. Each image must be processed and segmented individually, resulting in significant time consumption. Additionally, it is beyond the scope of this paper to dissect each module of image processing separately and evaluate its impact on the overall efficiency of the network.

However, this also underscores the need for further research. The validation performance of our proposed approach sees a significant decline when image enhancement is not employed. This implies that the overall efficacy of the model is reliant on image enhancement. However, it's important to note that this limitation isn't exclusive to our proposed method. To date, no efforts have been made to determine the optimal number of enhanced images. This aspect leaves room for future optimization of the efficiency of our proposed method.

V. Conclusions and Suggestions

The mortality rate associated with lung cancer remains alarmingly high, underscoring its status as one of the most prevalent and aggressive forms of cancer worldwide. While its occurrence cannot be prevented, early diagnosis can significantly improve patient outcomes, prolonging lives. Notably, in North America and other industrialized nations, lung cancer ranks as the leading cause of cancer-related deaths. Despite significant strides in recent years, early diagnosis remains challenging and lacks reliability.

In this study, we departed from current research trends to explore specialized layers within our CNN model. By integrating physiological data into our CNN model specifically designed for lung nodule classification, we achieved promising results. Our combined classifier attained an accuracy of 92.78%, surpassing similar models according to our literature review. Even in scenarios where feature learning layers may suffer from mistraining due to the absence of beneficial features, the classification accuracy of our proposed method remains reliable, thanks to the weighted aggregation of data collected from the medical body area network.

This study extends the development of one of the most precise automated models for lung cancer detection, emphasizing its comprehensive service availability. In summary, our proposed method represents a significant advancement in CNN-based automated models for lung cancer detection. We anticipate that our approach will pave the way for the development of more reliable computer-aided detection systems.

The proposed approach addresses the critical problem of early and accurate detection of lung cancer through the integration of data from CT scans and wearable IoT sensors, leveraging the DCNN for analysis. By combining information from both sources, the approach enhances diagnostic accuracy by capturing a comprehensive range of patient data. The hybrid model trained on a balanced dataset ensures robust learning and classification of lung nodules, while rigorous evaluation metrics such as accuracy, AUC score, loss, and recall provide thorough assessment of performance. Overall, the proposed approach offers a holistic and reliable solution to the challenge of lung cancer diagnosis, leveraging advanced machine learning techniques and diverse data sources to improve patient outcomes.

Future research could focus on integrating multi-modal data, including medical imaging, physiological data from wearable sensors, and patient history, into a comprehensive diagnostic model. By leveraging a wider range of data sources, such as genetic information, lifestyle factors, and environmental exposures, researchers can develop a more holistic understanding of lung cancer risk and improve the

accuracy of early detection models. This approach would require advanced data fusion techniques and machine learning algorithms capable of processing diverse data types and extracting meaningful patterns for accurate diagnosis and prognosis.

Another potential avenue for future research is the development of explainable artificial intelligence (XAI) models for lung cancer diagnosis. While deep learning models like CNNs have demonstrated impressive performance, their inner workings can be opaque, making it challenging to understand the factors driving their decisions. By incorporating explainability into the model architecture, researchers can provide clinicians with insights into how specific features contribute to the diagnostic process, enhancing trust and facilitating clinical decision-making. This research could involve exploring interpretable machine learning techniques, such as attention mechanisms, feature visualization, and decision trees, to create transparent and clinically actionable diagnostic models for lung cancer detection.

REFERENCES

[1] J. Kuruvilla and K. Gunavathi, "Lung cancer classification using neural networks for CT images," Comput Methods Programs Biomed, vol. 113, no. 1, pp. 202–209, 2014.

[2] B. P. Tripp, "Similarities and differences between stimulus tuning in the inferotemporal visual cortex and convolutional networks," in 2017 International Joint Conference on Neural Networks (IJCNN), IEEE, 2017, pp. 3551–3560.

[3] I. Durosini et al., "Patient preferences for lung cancer treatment: a qualitative study protocol among advanced lung cancer patients," Front Public Health, vol. 9, p. 622154, 2021.

[4] C. J. Chapman et al., "Autoantibodies in lung cancer: possibilities for early detection and subsequent cure," Thorax, vol. 63, no. 3, pp. 228–233, 2008.

[5] P. K. Shah et al., "Missed non–small cell lung cancer: radiographic findings of potentially resectable lesions evident only in retrospect," Radiology, vol. 226, no. 1, pp. 235–241, 2003.

[6] J.-F. Daneault et al., "Accelerometer data collected with a minimum set of wearable sensors from subjects with Parkinson's disease," Sci Data, vol. 8, no. 1, p. 48, 2021.

[7] J. Molimard, T. Delettraz, and E. Ojardias, "Development of a miniaturized motion sensor for tracking warning signs of low-back pain," arXiv preprint arXiv:2104.03565, 2021.

[8] J. Henderson, J. Condell, J. Connolly, D. Kelly, and K. Curran, "Review of wearable sensor-based health monitoring glove devices for rheumatoid arthritis," Sensors, vol. 21, no. 5, p. 1576, 2021.

[9] H. Teymourian, F. Tehrani, K. Mahato, and J. Wang, "Lab under the skin: microneedle based wearable devices," Adv Healthc Mater, vol. 10, no. 17, p. 2002255, 2021.

[10] L. Wang, K. Jiang, and G. Shen, "Wearable, implantable, and interventional medical devices based on smart electronic skins," Adv Mater Technol, vol. 6, no. 6, p. 2100107, 2021.

[11] K. A. G. Udeshani, R. G. N. Meegama, and T. G. I. Fernando, "Statistical feature-based neural network approach for the detection of lung cancer in chest x-ray images," International Journal of Image Processing (IJIP), vol. 5, no. 4, pp. 425–434, 2011.

[12] I. Bush, "Lung nodule detection and classification," Rep. Stanf. Comput. Sci, vol. 20, pp. 196–209, 2016.

[13] A. M. R. Schilham, B. Van Ginneken, and M. Loog, "A computer-aided diagnosis system for detection of lung nodules in chest radiographs with an evaluation on a public database," Med Image Anal, vol. 10, no. 2, pp. 247–258, 2006.

[14] B. Keserci and H. Yoshida, "Computerized detection of pulmonary nodules in chest radiographs based on morphological features and wavelet snake model," Med Image Anal, vol. 6, no. 4, pp. 431–447, 2002.

[15] M. A. Hussain, T. M. Ansari, P. S. Gawas, and N. N. Chowdhury, "Lung cancer detection using artificial neural network & fuzzy clustering," International journal of advanced research in computer and communication engineering, vol. 4, no. 3, pp. 360–363, 2015.

[16] N. Hadavi, M. J. Nordin, and A. Shojaeipour, "Lung cancer diagnosis using CT-scan images based on cellular learning automata," in 2014 International Conference on Computer and Information Sciences (ICCOINS), IEEE, 2014, pp. 1–5.

[17] S. Otte et al., "OCT A-Scan based lung tumor tissue classification with Bidirectional Long Short Term Memory networks," in 2013 IEEE International Workshop on Machine Learning for Signal Processing (MLSP), IEEE, 2013, pp. 1–6.

[18] X. Li and R. Wang, "A new efficient 2D combined with 3D CAD system for solitary pulmonary nodule detection in CT images," International Journal of Image, Graphics and Signal Processing, vol. 3, no. 4, p. 18, 2011.

[19] F. Taher and R. Sammouda, "Lung cancer detection by using artificial neural network and fuzzy clustering methods," in 2011 IEEE GCC conference and exhibition (GCC), IEEE, 2011, pp. 295–298.

[20] W. Shen et al., "Multi-crop convolutional neural networks for lung nodule malignancy suspiciousness classification," Pattern Recognit, vol. 61, pp. 663–673, 2017.

[21] W. Zhang, X. Wang, X. Li, and J. Chen, "3D skeletonization feature based computer-aided detection system for pulmonary nodules in CT datasets," Comput Biol Med, vol. 92, pp. 64–72, 2018.

[22] P. Wu, K. Xia, and H. Yu, "Correlation coefficient based supervised locally linear embedding for pulmonary nodule recognition," Comput Methods Programs Biomed, vol. 136, pp. 97–106, 2016.

[23] B. Kaliski, "Password-based cryptography specification," RFC 2898, 2000.

[24] A. Buades, B. Coll, and J.-M. Morel, "A non-local algorithm for image denoising," in 2005 IEEE computer society conference on computer vision and pattern recognition (CVPR'05), Ieee, 2005, pp. 60–65.

[25] U. K. Acharya and S. Kumar, "Genetic algorithm based adaptive histogram equalization (GAAHE) technique for medical image enhancement," Optik (Stuttg), vol. 230, p. 166273, 2021.

[26] W. J. Sori, J. Feng, and S. Liu, "Multi-path convolutional neural network for lung cancer detection," Multidimens Syst Signal Process, vol. 30, pp. 1749–1768, 2019.

[27] M. M. Prieto, E. Montanes, and O. Menendez, "Power plant condenser performance forecasting using a non-fully connected artificial neural network," Energy, vol. 26, no. 1, pp. 65–79, 2001.

[28] A. Mittal, A. P. Singh, and P. Chandra, "A modification to the Nguyen–Widrow weight initialization method," in Intelligent Systems, Technologies and Applications: Proceedings of ISTA 2018, Springer, 2019, pp. 141–153.

[29] P. Singh, "An extended framework of lung cancer classification using hybrid architecture of surf and svm," INFORMATION TECHNOLOGY IN INDUSTRY, vol. 9, no. 1, pp. 1489–1502, 2021.

[30] S. Yu et al., "Hessian-aware pruning and optimal neural implant," in Proceedings of the IEEE/CVF Winter Conference on Applications of Computer Vision, 2022, pp. 3880–3891.

[31] M. T. Hagan and M. B. Menhaj, "Training feedforward networks with the Marquardt algorithm," IEEE Trans Neural Netw, vol. 5, no. 6, pp. 989–993, 1994.

[32] E. M. Mustafa, M. A. Elshafey, and M. M. Fouad, "Accuracy enhancement of a blind image steganalysis approach using dynamic learning rate-based CNN on GPUs," in 2019 10th IEEE International Conference on Intelligent Data Acquisition and Advanced Computing Systems: Technology and Applications (IDAACS), IEEE, 2019, pp. 28–33.

[33] S. G. Armato III et al., "The lung image database consortium (LIDC) and image database resource initiative (IDRI): a completed reference database of lung nodules on CT scans," Med Phys, vol. 38, no. 2, pp. 915–931, 2011.

[34] S. G. Armato III et al., "LUNGx Challenge for computerized lung nodule classification: reflections and lessons learned," Journal of Medical Imaging, vol. 2, no. 2, 2015.

[35] R. Takahashi, T. Matsubara, and K. Uehara, "Ricap: Random image cropping and patching data augmentation for deep cnns," in Asian conference on machine learning, PMLR, 2018, pp. 786–798.

[36] K. Simonyan and A. Zisserman, "Very deep convolutional networks for large-scale image recognition In: Proceedings of International Conference on Learning Representations," 2015.

[37] O. Russakovsky et al., "Imagenet large scale visual recognition challenge," Int J Comput Vis, vol. 115, pp. 211–252, 2015.

[38] M. I. Mahmud, M. Mamun, and A. Abdelgawad, "A Deep Analysis of Transfer Learning Based Breast Cancer Detection Using Histopathology Images," in 2023 10th International Conference on Signal Processing and Integrated Networks (SPIN), IEEE, 2023, pp. 198–204.

[39] J. N. Mandrekar, "Receiver operating characteristic curve in diagnostic test assessment," Journal of Thoracic Oncology, vol. 5, no. 9, pp. 1315–1316, 2010.

[40] Dinesh Reddy, B., N. Thirupathi Rao, and Debnath Bhattacharyya. "Deep Neural Transfer Network Technique for Lung Cancer Detection." In Machine Intelligence Techniques for Data Analysis and Signal Processing: Proceedings of the 4th International Conference MISP 2022, Volume 1, pp. 237-247. Singapore: Springer Nature Singapore, 2023.

[41] Mohana Krishna, N., and R. Puviarasi. "Convolutional neural network based ResNet50 for finding accuracy in prediction of lung cancer using CT images and compared with CNN based inception V3." In AIP Conference Proceedings, vol. 2816, no. 1. AIP Publishing, 2024.